Electromagnetic Compatibility Analysis of PIND Equipment for Rocket Engine Attached Pipes

Guotao Wang[1,2(✉)], Qun Ding[1], Leizhen Gao[2], Qiang Wang[2], and Liang Guo[2]

[1] School of Electronic Engineering, Heilongjiang University, Harbin, China
star5892@163.com
[2] Reliability Institute for Electric Apparatus and Electronic, Harbin Institute of Technology, Harbin, China

Abstract. The remainders in attached pipelines of rocket engine are great harm to the reliable operation of engine. Signal noise and misjudgment caused by electromagnetic interference reduce the detection accuracy seriously. This paper analyzes the common-mode voltage of the rectifier bridge side and the inverter side of the detection equipment. According to the cut-off frequency, the fundamental voltage drop and the fundamental current and other parameters, the common-mode voltage filter is designed. The crosstalk coupling process between cable bundles is analyzed in this paper. Based on the finite element method, the distribution parameters of the cable bundle are analyzed and the structure of the cable bundle is optimized. With these methods, the impact of electromagnetic interference on the accuracy of remainders detection is reduced effectively.

Keywords: Attached pipelines of rocket engine · Remainder · PIND · Electromagnetic compatibility

1 Introduction

Remainder refers to all the material which exist in the product and has nothing to do with the requirement. It may be entered by external or internally generated [1]. Rocket engine as a power plant for aerospace systems, its reliability is a key factor in for the launch mission [2]. The structure of rocket engine is complex, and the assembly process is numerous, so remainders are not easy to be perceived. Free remainder will cause propel system exceptions, mechanical failure, control system damage and other

issues, even lead to casualties. Therefore, the detection of remainders in attached pipelines of rocket is a necessary measure to exclude rocket engine work failure.

2   Research Background

Based on Particle Impact Noise Detection (PIND), Harbin Institute of Technology designed automatic detection system for remainders in attached pipelines of rocket engine. The schematic diagram is shown in Fig. 1.
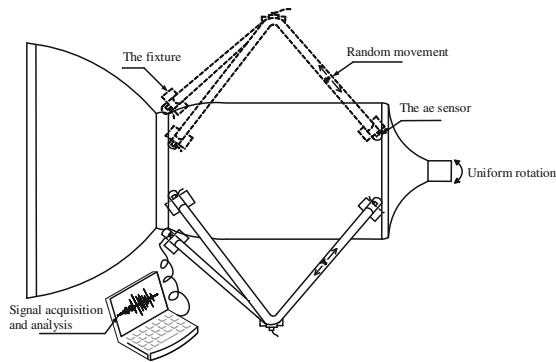

Fig. 1. The detection system of remainders in attached pipelines of rocket engine

2.1   Existing Problems

In order to provide sufficient and adjustable excitation capacity, the frequency conversion is employed. A lot of data show that the electromagnetic interference makes the background noise increased by 30%–55%. In addition, the electromagnetic interference increases detective complexity of remainder signal, and result in misjudgment.

The main problems of electromagnetic compatibility in this system are:

- As a result of PWM technology, the output pulse of inverter contains a large number of high-order harmonic components.
- The pulse output voltage generated by the high-speed power switching devices causes serious electromagnetic interference to the sensor.
- The power lines of motor and the signal lines of acoustic emission sensor pass through the center shaft, and crosstalk occurs between them.

2.2   Research Status at Home and Abroad

In the electromagnetic compatibility of the variable frequency drive system, B. Basavaraja proposed the improved second-order RLC low-pass filter [5]. A. Consoliand designed a four-phase inverter to eliminate the common-mode voltage, and proposed "auxiliary phase" and second-order LC filter [6]. Sun Li have studied the electromagnetic interference generated in the integration of electrical systems [7].

The methods of studying the electromagnetic compatibility of shielded cable mainly include the field method and the equivalent road method. Taylor put forward a variety of field-line coupling model, and domestic research is mainly based on transmission line theory [8]. Sun Beiyun proposed the calculation of the distributed capacitance of the Multi-conductor cable [9]. Yi Bin study the coupling response of voltage and current in the shielded cable with ANSYS [10].

At present, there are few studies on the electromagnetic interference in the detection of remainders in attached pipelines of rocket engine, so it needs further analysis.

3 Electromagnetic Compatibility Analysis of Variable Frequency Drive System

The variable frequency drive system is composed of frequency converter and asynchronous motor, the IGBT in the inverter circuit produce a higher common-mode voltage [11], which is the main source of electromagnetic interference. The simulation schematic diagram of variable frequency drive system is shown in Fig. 2.
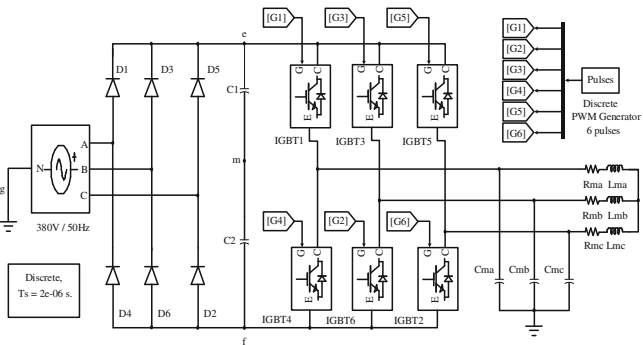

Fig. 2. Simulation schematic diagram of variable frequency drive system

3.1 Common-Mode Voltage of the Rectifier Bridge

From Fig. 2, the function is as follows:

$$U_{mg} = \frac{U_{eg} + U_{fg}}{2} \tag{1}$$

$$U_{mg} = \frac{3\sqrt{2}}{8\pi} U_{AB} \sin(3wt) + \frac{3\sqrt{2}}{80\pi} U_{AB} \sin(9wt) + \ldots \tag{2}$$

The Fourier series expansion formula in (2) [12]. Where w is the fundamental frequency of AC input voltage, and U_{AB} is the AC input line voltage.

The model of variable frequency drive system is established by Simulink, the waveform and spectrum of U_{mg} are shown in Fig. 3. There is $6k - 1$ (k = 1, 2, 3,...)

harmonics, where there is no harmonics at the fundamental frequency, the amplitude of the third harmonic is the largest and the amplitude of the harmonics decreases with increasing frequency.
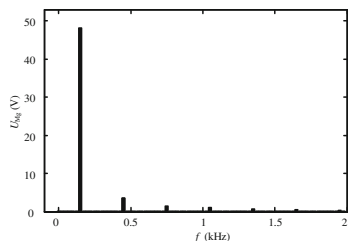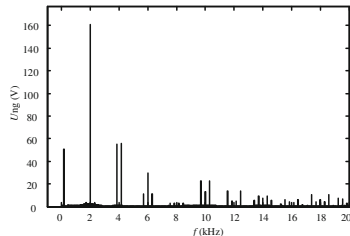

Fig. 3. Original waveform spectrum

Fig. 4. New spectrum

3.2 Common-Mode Voltage of the Inverter

Figure 4 shows the simulation waveform of the common-mode voltage. The Fourier expression of the common-mode voltage U_{ng} is as follows [12]:

when $n = 1, 3, 5,\ldots, k = 6j, j = 1, 2, 3, \ldots$

$$U_{ng} = \sum_{n=1}^{\infty} (-1)^{(n-1)/2} \frac{E_{DC}}{2} \left(\frac{4}{n\pi}\right) \left\{ J_0\left(\frac{an\pi}{2}\right) \cos(nw_s t) + 3 \sum_{n=1}^{\infty} J_k\left(\frac{an\pi}{2}\right) [\cos(nw_s + kw_1)t + \cos(nw_s - kw_1)t] \right\} \quad (3)$$

when $n = 2, 4, 6,\ldots, k = 6j - 3, j = 1,2,3,\ldots$

$$U_{ng} = 3 \sum_{n=1}^{\infty} (-1)^{n/2} \frac{E_{DC}}{2} \left(\frac{4}{n\pi}\right) J_k\left(\frac{an\pi}{2}\right) [\sin(nw_s + kw_1)t + \sin(nw_s - kw_1)t] \quad (4)$$

Where w_s is the carrier angular frequency, w_1 is the modulation wave angular frequency, J_k is the k-order Bessel function, and E_d is the DC bus voltage.

From (3), (4) and Fig. 6, if the modulated wave is the sine wave, w_1 of the modulation wave does not exist in the common-mode voltage. The harmonics will exist only when the carrier frequency is odd times of w_s, and the harmonic amplitude of the double carrier is largest. The inter-harmonics exists at the frequency $nw_s \pm kw_1$.

3.3 Design of Common-Mode Voltage Filter for Three-Phase Inverter

As shown in Fig. 5, this paper selects the second order RLC passive filter to suppress the differential mode voltage and the common mode voltage. The model parameters of the induction motor as follows: R_{ma} is 22Ω, L_{ma} is 44 mH, C_{ma} is 6nF.

The common-mode voltage of the inverter:

$$U_{ng} = \frac{V_1 + V_2 + V_3}{3} = \frac{V_{1m} + V_{2m} + V_{3m}}{3} + V_{mg} \tag{5}$$

From circuit analysis:

$$U_{ng} = \frac{1}{3}\left(R_f i_o + \frac{1}{C_f}\int i_o dt\right) + U_{fm} + U_{mn} \tag{6}$$

According to (6), U_{ng} is proportional to R_f, inversely proportional to C_f. The filter parameters can be determined synthetically by cutoff frequency, fundamental voltage drop, fundamental current [13].
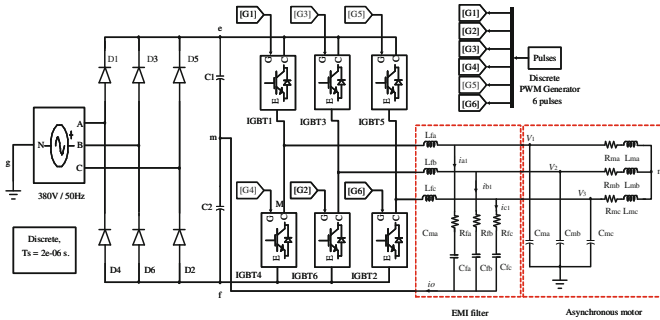

Fig. 5. Simulation schematic of variable frequency drive system with filter

- **Cut-off frequency.** The harmonic amplitude of the common-mode voltage is largest at the carrier frequency. And, the cutoff frequency should less than one tenth of carrier frequency. If the operating frequency of the filter is too low, it will bring the capacitor current and phase shift. Therefore, the cutoff frequency is usually ten times higher than fundamental frequency. Considering the conditions and verified by experiments, the cut-off frequency is determined to be 400 Hz.
- **Filter inductance.** Usually the fundamental voltage drop on the inductor should be less than 3% $\sim$ 5%, the inductance range is

$$L_f = (3\% \sim 5\%)L_{ma} = 1.32\,\text{mH} \sim 2.2\,\text{mH, select } L_f = 1.6\,\text{mH.}$$

- **Filter capacitor.** In the no-load conditions, the fundamental current of the capacitance should be less than 10% of the inverter output current, the inverter rated current is 30A, rated power $E_d = 17.5$ kW. Then $I_c = aE_d \pi fC/\sqrt{2} = 3$A, and the solution is 1.54 μF.
- **Damping resistance.** Too large value of resistance will affect the dead time of switch. In addition, the capacitor capacitance is less than 20% of the rated current of

the inverter when circuit modulates. Considering the conditions and after simulating and experimenting, select $R_f = 2\Omega$.

The simulation results are shown in Fig. 6 to Fig. 8. From Figs. 4 and 6, the high-frequency common-mode voltage of 2 kHz or more is well suppressed after filtered. Figures 7 and 8 show that it also has a good effect on differential mode voltage.
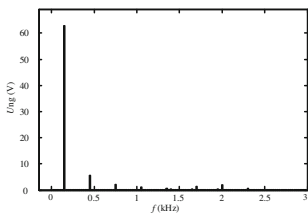

Fig. 6. Common voltage spectrum of filtered inverter
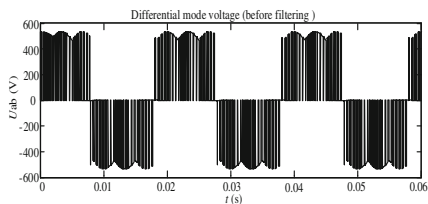
Fig. 7. mode voltage before filtering
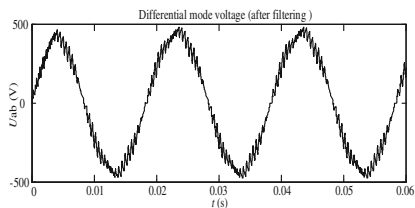
Fig. 8. mode voltage after filtering

4   Electromagnetic Compatibility Analysis of Sensor Cable

4.1   Coupling Theory of Capacitance and Inductance

The electromagnetic energy causes crosstalk when the distributed capacitance and the distributed inductance are coupled. The capacitive coupling between the cables is:

$$U_2 = \frac{Z_i}{Z_i + \frac{1}{\mathrm{j}wc}} U_i \tag{7}$$

(7) displays that the electromagnetic interference voltage U_2 is related to the value of coupling capacitance C and input impedance Z_i, and decreasing the values of w, C and Z_i can reduce the electromagnetic interference caused by the capacitive coupling.

The inductance coupling between the cables is:

$$U_{\mathrm{N}} = \frac{\mathrm{d}}{\mathrm{d}t}MI_1 = M\frac{\mathrm{d}}{\mathrm{d}t}I_1 = \mathrm{j}wMI_1 \tag{8}$$

(8) shows U_{N} is proportional to $\mathrm{d}I_1/\mathrm{d}t$ and M, therefore reducing M and decreasing the frequency w can suppress the inductance coupling voltage [10].

4.2   Finite Element Analysis of the Sensor Cable

Based on the finite element principle, this paper calculates the distribution parameters between cables.
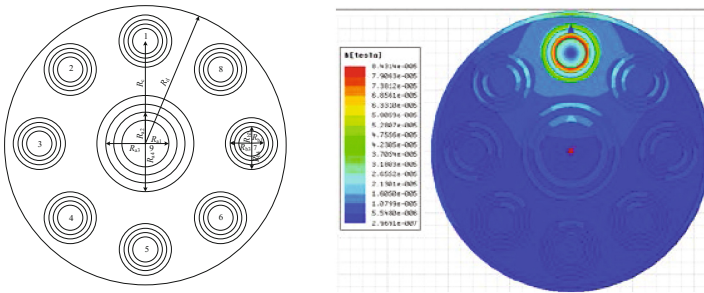

Fig. 9. Cable simulation diagram

Figure 9 shows the 9-conductor cable model that is established by the Maxwell. Each wire is composed of core layer, inner insulating layer, shielding layer and outer insulating layer from inside to outside. According to the actual cable, the relative permittivity of the inner and outer insulating layers and the intermediate filling layer is set to 2.5, 2.6 and 2.1. The relative permeability of all the media is 1, the structural parameters are as follows: $R_{a1} = 3$ mm, $R_{a2} = 4$ mm, $R_{a3} = 5$ mm, $R_{a4} = 6$ mm, $R_{b1} = 1$ mm, $R_{b2} = 1.5$ mm, $R_{b3} = 2$ mm, $R_{b4} = 2.5$ mm, $R_c = 9.5$ mm, $R_d = 13$ mm.

By calculating the distributed capacitance and inductance between the cables, It can be seen from Tables 1 and 2, the distributed capacitance between the sensor cores is 0 when the shield is applied, and it exists only between the shielding layers and the sensor cables. Without shielding, there is a pF-level capacitance. If the shielding layer is applied, the self- capacitance is calculated in the reference system, so the self-capacitance value is larger than that without shielding layer.

Table 1. Capacitance simulation results with shielding layer (pF)

C	1	2	3	9	10	16	17	18
1	137.22	0	0	0	0	0	0	0
2	0	137.22	0	0	0	0	0	0
3	0	0	137.22	0	0	0	0	0
:	:	:	:	:	:	:	:	:
9	0	0	0	139.39	−139.39	0	0	0
10	0	0	0	−139.39	310.3	−14.598	−14.598	−14.598
11	−137.22	0	0	0	−14.598	−0.2083	−0.6506	−12.152
12	0	−137.22	0	0	−14.598	−0.1301	−0.2084	−0.6507
13	0	0	−137.22	0	−14.598	−0.2084	−0.1301	−0.2085
14	0	0	0	0	−14.598	−0.6507	−0.2085	−0.1301
15	0	0	0	0	−14.598	−12.15	−0.6507	−0.2085
16	0	0	0	0	−14.598	180.62	−12.15	−0.6501
17	0	0	0	0	−14.598	−12.15	180.62	−12.15
18	0	0	0	0	−14.598	−0.6501	−12.15	180.62

Table 2. Capacitance simulation results without shielding layer (pF)

C	1	2	3	4	5	6	7	8	9
1	23.92	−6.600	−0.838	−0.294	−0.238	−0.294	−0.838	−6.600	−5.972
2	−6.600	23.92	−0.838	−0.838	−0.838	−0.294	−0.294	−0.838	−5.972
3	−0.838	−6.600	23.92	−6.600	−0.838	−0.294	−0.238	−0.294	−5.972
4	−0.294	−0.838	−6.600	23.92	−6.600	−6.600	−0.294	−0.238	−5.972
5	−0.238	−0.294	−0.838	−6.600	23.92	6.600	−0.838	−0.294	−5.972
6	−0.294	−0.238	−0.294	−0.838	−6.600	23.92	−6.600	−0.838	−5.972
7	−0.838	−0.294	−0.238	−0.294	−0.838	−6.600	23.92	−6.600	−5.972
8	−6.600	−0.838	−0.294	−0.238	−0.294	−0.838	−6.600	23.92	−5.972
9	−5.972	−5.972	−5.972	−5.972	−5.972	−5.972	−5.972	−5.972	48.521

5 Conclusion

This paper analyzes the principle of generating electromagnetic interference in the variable frequency transmission system and multicore pin cable in the automatic detection system of remainders in attached pipelines of rocket engine, and simulates the common mode voltage of the inverter and the distribution parameters of the cable. The main conclusions are as follows. The mechanism and characteristics of the common mode voltage of the rectifier and the inverter are analyzed. RLC passive filter is designed to suppress the common mode voltage. The principle of crosstalk between sensor cables is analyzed, and the simulation model of 9-conductor cable is established.

References

1. QJ 2850-1996: Prevention and control for foreign object debris (FOD) of space products. Beijing: Commission of Science, Technology and Industry for National Defense (1996)
2. Lu, X.: Inexhaustible power that recommend the "Long March" rocket - the development of "Long March" rocket engine in aerospace propulsion technology research institute. Aerosp. Indus. Manage. **6**, 18–22 (2007)
3. Zhen, X., et al.: Current analysis of remainder's control in rocket testing proces. J. Sichuan Ordnance **36**(6), 74–76 (2015)
4. Qin, Y., et al.: Method of man-machine-environment control over foreign object debris in pipelines used in rocket engine test. J. Rocket Propul. **41**(6), 80–85 (2015)
5. Basavaraja, B., Siva Sarma, D.V.S.S.: Modeling and simulation of dv/dt filters for AC drives with fast switching transients. In: Power India Conference IEEE, pp. 10–14 (2006)
6. Consoli, A., et al.: An innovative EMI reduction design technique in power converters. IEEE Trans. Electromagn. Compat. **38**(4), 567–575 (1996)
7. Sun, L., Nie, J.: Analysis of electromagnetic compatibility in integrated motor system. Servo Control **6**, 33–35 (2010)
8. Wang, C., Zhu, C.: The present research and development trend of electromagnetic fields coupling to shielding cables. Electr. Wire Cable **3**, 1–5 (2011)
9. Sun, B., et al.: Method of moment for calculating capacitance of shielded multiconductor cable. High Power Laser Part. Beams **12**(6), 749–752 (2000)
10. Yi, B., Wang, Z.: Parameters calculation of shield cable and crosstalk between shielding layer and core wires. High Voltage Eng. **34**(4), 804–808 (2008)
11. Dai, S., et al.: Design of common-mode and differential-mode voltage dv/dt filter at inverter output terminals. Chin. J. Power Sources **39**(9), 1985–1988 (2015)
12. Jiang, Y., et al.: Research on common-mode voltage generated by a PWM inverter and its cancellation technology. Proc. CSEE **25**(9), 47–53 (2005)
13. Yan, B., Chen, X.: The engineering design of VVVF output PLC sine-wave filter. Electr. Mach. Control **6**(3), 256–260 (2002)